Synthesis and Characterization of Amphiphilic Phenylene Ethynylene Oligomers and Their Langmuir−Blodgett Films

Zhexiong Tang,† Raea K. Hicks,† Rudolph J. Magyar,‡ Sergei Tretiak,‡ Yuan Gao,*,† and Hsing-Lin Wang*,†

PCAS, Chemistry Division, and Theoretical Division, Los Alamos National Laboratory, Los Alamos, New Mexico 87545

Received April 5, 2006. In Final Form: July 13, 2006

We report the synthesis of a series of amphiphilic molecular building blocks that can be self-assembled at the air−water interface to form two- and three-dimensional nanostructures with tunable optoelectronic properties. Compression of these molecular building blocks using the Langmuir−Blodgett method gives rise to monolayer and multilayer thin films with different packing densities and electronic properties that are tunable due to varying $\pi-\pi$ (hydrophobic) interactions. Depending on the noncovalent interaction between chromophores, we observe a transition toward denser packing with increasing number of phenylene ethynylene repeat units. Additionally, we use quantum-chemical simulations to help determine the excited-state electronic structure, intermolecular interactions, and packing trends. Our results demonstrate that the interplay between dipole−dipole and $\pi-\pi$ interactions dominates the formation of thin films with various packing densities and determines the associated optical properties.

Introduction

Conjugated polymers and oligomers are currently the compounds that are most widely used for the construction of electronic and optical devices.[1−3] The year 1990 brought the first report of an electroluminescent device made from poly(phenylenevinylene) (PPV),[4] and with the next half-decade, emitting layers in similar constructions were made from other conjugated polymers such as poly(*p*-phenylene) (PPP)[5] and poly(thiophene).[6] Poly(phenylene ethynylene) (PPE)s and oligomeric phenylene ethynylene (OPE)s are acetylene analogues of PPV that are based on the phenyl ethynyl unit. Their rigid rodlike character and conjugation[7,8] are properties that have made them useful as light-emitting diodes,[9,10] plastic lasers,[11] light-emitting electrochemical cells,[12,13] and polarizers in liquid crystal displays.[14]

Furthermore, branching of linear chains produces tree-like molecules (dendrimers) that may be used to extend desirable electronic properties even further.[15,16] In particular, dendrimers are believed to be promising building blocks for artificial light-harvesting systems.[17−19]

OPEs are based on the same repeat unit as PPEs. They are monodisperse and shape-persistent,[1] which makes them valuable for the fabrication of molecular electronics. It has been suggested that single or small packets of molecules may function as the active channels for information transportation, processing, and storage.[20−23] However, the understanding of the underlying mechanisms that dictate formation of self-assembled monolayers and multilayers of thin films based on OPEs remains primitive, despite the extensive efforts toward investigating the electronic properties of the OPEs' molecular structures.[24] Considering the importance of phenylene ethynylene-based materials and its analogues in fabricating thin film devices, it is very important to look into how these molecules come together to form high-dimensional materials by way of self-assembly and to understand their structure−property relationship. Doing so will bring more controllability to the properties of electronics based on these molecules.

Well-ordered thin films made by the Langmuir−Blodgett (LB) technique can reveal structure−property relationships when they are characterized by a combination of spectroscopy probes such as UV−vis, ellipsometry, fluorescence, X-ray, and neutron

* Corresponding authors. E-mail: yuangao@lanl.gov (Y.G.); hwang@lanl.gov (H.-L.W.).

† Chemistry Division.

‡ Theoretical Division.

(1) Tour, J. M. *Chem. Rev.* **1996**, *96*, 537−553.
(2) Scherf, U. *Carbon Rich Compd. II* **1999**, *201*, 163−222.
(3) Segura, J. L.; Martin, N. *J. Mater. Chem.* **2000**, *10*, 2403−2435.
(4) Burroughes, J. H.; Bradley, D. D. C.; Brown, A. R.; Marks, R. N.; Mackay, K.; Friend, R. H.; Burns, P. L.; Holmes, A. B. *Nature* **1990**, *347*, 539−41.
(5) Grem, G.; Leditzky, G.; Ullrich, B.; Leising, G. *Adv. Mater.* **1992**, *4*, 36−7.
(6) Berggren, M.; Inganas, O.; Gustafsson, G.; Rasmusson, J.; Andersson, M. R.; Hjertberg, T.; Wennerstrom, O. *Nature* **1994**, *372*, 444−6.
(7) Yang, J. S.; Swager, T. M. *J. Am. Chem. Soc.* **1998**, *120*, 5321−5322.
(8) Weder, C.; Wrighton, M. S. *Macromolecules* **1996**, *29*, 5157−5165.
(9) Neher, D. *Adv. Mater.* **1995**, *7*, 691−702.
(10) Kraft, A.; Grimsdale, A. C.; Holmes, A. B. *Angew. Chem., Int. Ed.* **1998**, *37*, 402−428.
(11) Hide, F.; Diazgarcia, M. A.; Schwartz, B. J.; Heeger, A. J. *Acc. Chem. Res.* **1997**, *30*, 430−436.
(12) Pei, Q. B.; Yu, G.; Zhang, C.; Yang, Y.; Heeger, A. J. *Science* **1995**, *269*, 1086−1088.
(13) Blom, P. W. M.; Dejong, M. J. M.; Vleggaar, J. J. M. *Appl. Phys. Lett.* **1996**, *68*, 3308−10.
(14) Weder, C.; Sarwa, C.; Montali, A.; Bastiaansen, G.; Smith, P. *Science* **1998**, *279*, 835−7.
(15) Percec, V.; Glodde, M.; Bera, T. K.; Miura, Y.; Shiyanovskaya, I.; Singer, K. D.; Balagurusamy, V. S. K.; Heiney, P. A.; Schnell, I.; Rapp, A.; Spiess, H. W.; Hudson, S. D.; Duan, H. *Nature* **2002**, *419*, 384−7.
(16) Yaliraki, S. N.; Ratner, M. A.; Aviram, A.; Ratner, M.; Mujica, V. Interplay of Topology and Chemical Stability on the Electronic Transport of Molecular Junctions. *Ann. N.Y. Acad. Sci.*; New York Academy of Sciences: New York, 2002; pp 153−162.
(17) Gilat, S. L.; Adronov, A.; Frechet, J. M. J. *Angew. Chem., Int. Ed.* **1999**, *38*, 1422−1427.
(18) Kopelman, R.; Shortreed, M.; Shi, Z. Y.; Tan, W. H.; Xu, Z. F.; Moore, J. S.; Barhaim, A.; Klafter, J. *Phys. Rev. Lett.* **1997**, *78*, 1239−42.
(19) Tretiak, S.; Chernyak, V.; Mukamel, S. *J. Phys. Chem. B* **1998**, *102*, 3310−3315.
(20) Le Moigne, J.; Gallani, J. L.; Wautelet, P.; Moroni, M.; Oswald, L.; Cruz, C.; Galerne, Y.; Arnault, J. C.; Duran, R.; Garrett, M. *Langmuir* **1998**, *14*, 7484−92.
(21) Tour, J. M.; Reinerth, W. A.; Jones, L.; Burgin, T. P.; Zhou, C. W.; Muller, C. J.; Deshpande, M. R.; Reed, M. A. Conference on Molecular Electronics−Science and Technology; December 14−18, 1997; *Ann. N.Y. Acad. Sci.* **1998**, *852*, 197−204.
(22) Tour, J. M. *Acc. Chem. Res.* **2000**, *33*, 791−804.
(23) Reed, M. A.; Tour, J. M. *Sci. Am.* **2000**, *282*, 86−93.
(24) Magyar, R. J.; Tretiak, S.; Gao, Y.; Wang, H. L.; Shreve, A. P. *Chem. Phys. Lett.* **2005**, *401*, 149−56.

10.1021/la060914k CCC: $33.50
Published on Web 09/06/2006

Scheme 1. Synthetic Scheme of Amphiphilic Phenylene−Ethynylene Dimer, Trimer, and Tetramer

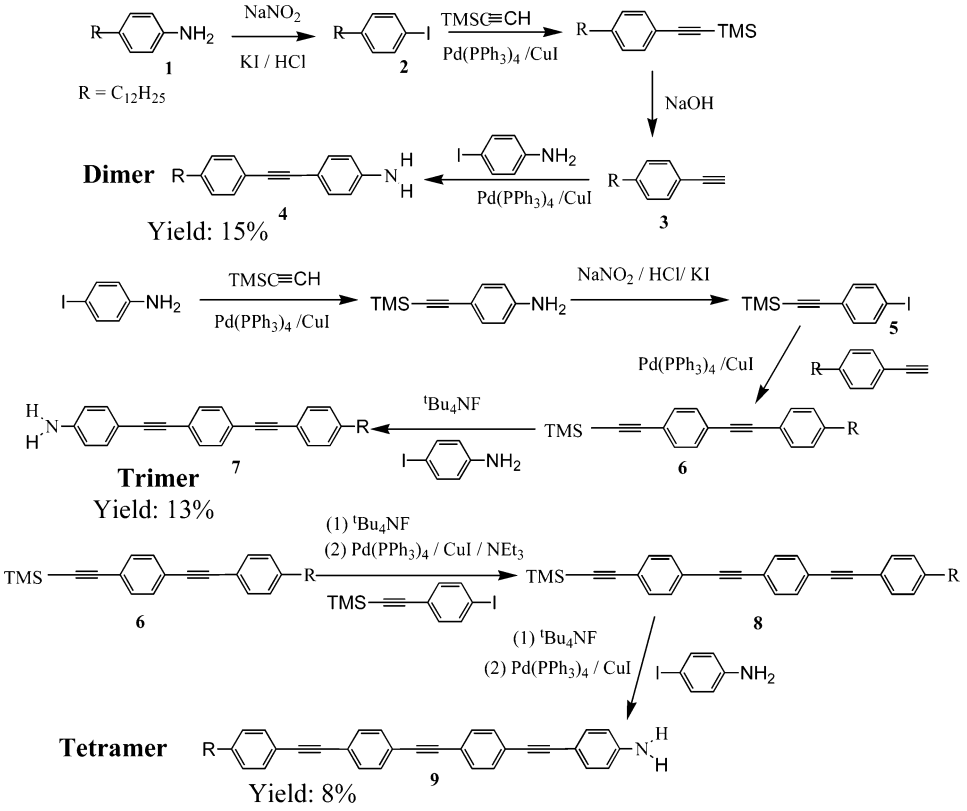

scattering. The technique involves floating small amounts of the molecule on a water subphase, compressing the layer to form a two-dimensional "solid", and transferring the "solid" onto a substrate. Unfortunately, OPEs are not usually suited for this sort of study due to their nonamphiphilic nature and tendency to aggregate caused by strong $\pi-\pi$ interactions between oligomer backbones. In addition, the resulting Langmuir films are usually too rigid to be transferred satisfactorily onto solid substrates. Recently, Arias-Marin et al. successfully prepared Y-type LB films using side-chain amphiphilic phenylene ethynylene oligomers.[25] These amphiphiles lay flat at the air−water interface and hence occupy a large surface area (∼150−190 Å^2/molecule) and exhibit weak intermolecular interactions. Subsequently, they have demonstrated fabrication of LED devices with a quantum efficiency of $\sim 10^{-3}$% based on these amphiphiles.[25] They also synthesized a series of amphiphilic aryl−ethynylene homopolymers with amphiphilic character. These homopolymers give stable Langmuir films on the air−water interface, and the LB films can be transferred onto substrate surfaces.[26] The intrinsic quantum efficiency of phenylene ethynylene thin films relates strongly to the packing density and the aggregated phase. Earlier work by Kim et al. demonstrated controlled synthesis of PPE Langmuir and Langmuir−Blodgett films; these thin films reveal the interrelationship of the intrinsic optical properties of PPE derivatives and a single chain's conformation and/or interpolymer interactions, which provide insights for the development of highly emissive phenylene ethynylene thin films.[27−29]

Here, we report the synthesis of a series of amphiphilic phenylene ethynylene oligomers by attaching a strong hydrophilic headgroup and strong hydrophobic endgroup to the phenylene ethynylene dimer, trimer, and tetramer (Scheme 1). These phenylene ethynylene amphiphiles differ from the previously reported side-chain amphiphiles in that they stand perpendicular to the water surface while the molecules are being compressed to form a Langmuir thin film. Our amphiphiles also form densely packed monolayers at the air−water interface, and the monolayer can be transferred to a solid substrate to form mono- and multilayered LB films. Physical and optical characteristics of these films were determined from pressure isotherm, UV−vis, and fluorescence spectroscopy. Our results show that increasing $\pi-\pi$ interactions between oligomers leads to higher packing density in thin films and that physical and optical properties depend on the packing density. The packing density is tunable by changing the subphase pH and ionic strength. First-principle-based quantum-chemical calculations of PPE oligomers and their pairs rationalize observed experimental trends and help to validate our results. The understanding achieved through the modeling work shows promise for predicting and controlling the electronic and optical properties of the phenylene ethynylene self-assemblies.

Experimental Section

Synthesis. A detailed synthetic scheme of amphiphilic phenylene ethynylene oligomers using Pd catalyst is shown in Scheme 1. The syntheses involving the use of Pd $(PPh_3)_4$/CuI were performed under an argon atmosphere using standard Schlenk techniques. Solvents for these reactions were dried and purified using standard procedures. $Pd(PPh_3)_4$, CuI, 4-dodecylaniline, and 4-iodoaniline were purchased from Aldrich and used without further purification. 4-Ethynyldodecanebenzene **3** and 4-trimethylsilylethynyl iodobenzene **5** were

(25) Arias-Marin, E.; Arnault, J. C.; Guillon, D.; Maillou, T.; Le Moigne, J.; Geffroy, B.; Nunzi, J. M. *Langmuir* **2000**, *16*, 4309−18.
(26) Arias-Marin, E.; Le Moigne, J.; Maillou, T.; Guillon, D.; Moggio, I.; Geffroy, B. *Macromolecules* **2003**, *36*, 3570−3579.
(27) Deans, R.; Kim, J.; Machacek, M. R.; Swager, T. M. *J. Am. Chem. Soc.* **2000**, *122*, 8565−8566.
(28) Kim, J.; Swager, T. M. *Nature* **2001**, *411*, 1030−4.
(29) Kim, J.; Levitsky, I. A.; Mcquade, D. T.; Swager, T. M. *J. Am. Chem. Soc.* **2002**, *124*, 7710−7718.

synthesized according to the literature methods.[2,30] NMR spectra were recorded at room temperature with a Bruker 500 MHz spectrometer. FT-IR spectra were recorded with a Mattson spectrometer.

Synthesis of Dimer 4. To a solution of **3** (52.7 mg, 0.195 mmol), 4-iodoaniline (42.7 mg, 0.195 mmol), $Pd(PPh_3)_4$ (7 mg, 3 mol %), and CuI (2.2 mg, 6 mol %) in dry THF was added Et_3N (1 mL, excess). After the mixture was stirred at room temperature for 16 h, the solvent was evaporated and the residue was extracted with diethyl ether. After evaporation, the crude product was purified by column chromatography on silica gel with hexane/ethyl acetate (2:1) as eluent. Yield: 60%. IR (film, ν/cm^{-1}): 3469, 3377 (s, NH_2), 2208 (s, C≡C). ^{1}H NMR ($CDCl_3$): δ = 7.4 (m, 2H, Ph−H), 7.35 (m, 2H, Ph−H), 7.15 (m, 2H, Ph−H), 6.55 (m, 2H, Ph−H), 3.9 (br s, 2H, NH_2), 2.6 (m, 2H, Ar−CH_2), 1.3 (m, 20H, CH_2), 0.9 (m, 3H, CH_3).

Synthesis of the Precursor TMS−CC−C_6H_4−CC−C_6H_4−$C_{12}H_{25}$, 6. To a solution of **3** (350 mg, 1.29 mmol), **5** (390 mg, 1.3 mmol), $Pd(PPh_3)_4$ (30 mg, 2 mol %), and CuI (9 mg, 4 mol %) in dry THF (15 mL) was added Et_3N (2 mL, excess). After the mixture was stirred at room temperature for 16 h, the solvent was evaporated and the residue was extracted with diethyl ether. After evaporation, the crude product was purified by column chromatography on silica gel with hexane as eluent. Yield: 62%. IR (film, ν/cm^{-1}): 2156 (C≡C). ^{1}H NMR ($CDCl_3$): δ = 7.5 (m, 6H, Ph−H), 7.3 (m, 2H, Ph−H), 2.7 (m, 2H, Ar−CH_2), 1.3 (m, 20H, CH_2), 0.9 (m, 3H, CH_3), 0.25 (s, 9H, TMS).

Synthesis of Trimer 7. To a suspension of *t*-Bu_4NF and silica (1 g, 1 mmol) in dry methylene chloride (30 mL) was slowly added a solution of **6** (0.11 g, 0.25 mmol) in CH_2Cl_2 (10 mL). The mixture was stirred at room temperature for 30 min, and the solution was filtered. The silica was washed with CH_2Cl_2 several times. The combined organic solution was washed with aqueous $KHCO_3$, dried with $MgSO_4$, and the solvent was then removed under vacuum. To the solution of this material in THF (20 mL) were added 4-iodoaniline (54.7 mg, 0.25 mmol), $Pd(PPh_3)_4$ (8.4 mg, 0.0073 mmol), CuI (3.6 mg, 0.014 mmol), and Et_3N (1 mL, excess) in sequence. The mixture was stirred at room temperature for 16 h, the solvent was evaporated, and the residue was extracted with diethyl ether. After evaporation of the solvent, the crude product was purified by column chromatography on silica gel with hexane/ethyl acetate (2:1) as eluent. Yield: 40%. IR (film, ν/cm^{-1}): 3330 (br s, NH_2), 2220 (w s, C≡C). ^{1}H NMR ($CDCl_3$): δ = 7.5, 7.4, 7.2 (m, 10H, Ph−H), 6.7 (m, 2H, Ph−H), 3.9 (br s, 2H, NH_2), 2.6 (m, 2H, Ar−CH_2), 1.3 (m, 20H, CH_2), 0.9 (m, 3H, CH_3).

Synthesis of the Precursor TMS−CC−C_6H_4−CC−C_6H_4−CC−C_6H_4−$C_{12}H_{25}$, 8. To a suspension of *t*-Bu_4NF/silica (0.8−1.2 mmol) in methylene chloride (15 mL) was slowly added a solution of **6** (55 mg, 0.125 mmol) in CH_2Cl_2 (10 mL). The mixture was stirred at room temperature for 30 min and was then filtered. The silica was washed with CH_2Cl_2 several times (3 × 10 mL), and the combined organic solution was washed with aqueous $KHCO_3$ and dried with $MgSO_4$. The solvent was removed under vacuum, and the material obtained was used directly for the following reaction without further purification.

To a mixture of the material obtained above, **5** (37.5 mg, 0.125 mmol), $Pd(PPh_3)_4$ (4.2 mg, 3 mol %), and CuI (2 mg, 6 mol %) in dry THF (15 mL) was added Et_3N (1 mL, excess). After the mixture was stirred at room temperature for 16 h, the solvent was evaporated and the residue was extracted with diethyl ether. After evaporation, the crude product was purified by column chromatography on silica gel with hexane as eluent. Yield: 35%. IR (film, ν/cm^{-1}): 2156 (C≡C). ^{1}H NMR ($CDCl_3$): δ = 7.5 (m, 10H, Ph−H), 7.2 (m, 2H, Ph−H), 2.6 (m, 2H, Ar−CH_2), 1.3 (m, 20H, CH_2), 0.9 (m, 3H, CH_3), 0.25 (s, 9H, TMS).

Synthesis of Tetramer 9. To a suspension of *t*-Bu_4NF and silica (1 g, 1 mmol) in dry methylene chloride (30 mL) was slowly added a solution of **8** (20 mg, 0.033 mmol) in CH_2Cl_2 (10 mL). The mixture was stirred at room temperature for 30 min, and the solution was filtered. The silica was washed with CH_2Cl_2 several times. The combined organic solution was washed with aqueous $KHCO_3$, dried with $MgSO_4$, and the solvent was then removed under vacuum. To the solution of this material in THF (20 mL) were added 4-iodoaniline (7.12 mg, 0.033 mmol), $Pd(PPh_3)_4$ (1 mg, 0.0009 mmol), CuI (0.4 mg, 0.0018 mmol), and Et_3N (0.3 mL, excess) in sequence. The mixture was stirred at room temperature for 16 h, the solvent was evaporated, and the residue was extracted with diethyl ether. After evaporation of the solvent, the crude product was purified by column chromatography on silica gel with hexane/ethyl acetate (2:1) as eluent. Yield: 32%. IR (film, ν/cm^{-1}): 3320 (br s, NH_2), 2226 (w s, C≡C). ^{1}H NMR ($CDCl_3$): δ = 7.5, 7.4, 7.2 (m, 14H, Ph−H), 6.7 (m, 2H, Ph−H), 3.9 (br s, 2H, NH_2), 2.6 (m, 2H, Ar−CH_2), 1.3 (m, 20H, CH_2), 0.9 (m, 3H, CH_3).

Self-Assembly at the Air−Water Interface. First, 4.0×10^{-3} mmol of phenylene ethynylene oligomers was dissolved in 10 mL of chloroform to obtain 0.4 mM solutions of dimer, trimer, and tetramer. Next, 0.5 mL of these as-prepared chloroform solutions was spread on the water surface. The measurements of the surface pressure−area (Π−A) isotherms were carried out using a KSV 2000 standard L−B trough (KSV Instrument, Helsinki, Finland) with a Wilhelmy-type balance, Teflon trough, and symmetrical hydrophilic Delrin barriers. The complete system was controlled via a computer. The trough was set in an enclosure to be protected from dust and drafts, and the subphase temperature was controlled to within ±0.5 °C. Ultrapure water (resistivity greater than 18 MΩ cm) from a Barnstead e-pure system was used as the subphase. Monolayers were spread from chloroform solutions on an ultrapure water subphase at 21 °C. After waiting 30 min to allow solvent evaporation, we obtained isotherms by reducing the surface area available to the material at a rate of 10 mm/min. During the depositions, the transfer surface pressure was fixed at 25 mN m^{-1}.

All substrates were cleaned by immersion in a 7:3 mixture of concentrated sulfuric acid and 30% H_2O_2 at 80 °C for 1 h (Piranha etch treatment). Piranha solution is highly corrosive, very energetic, and potentially explosive. It should be handled with extreme caution at all times.

Prior to use, substrates were treated with octadecyltrichlorosilane (OTS, 1% in hexadecane solution) at 40 °C for 45 min and washed thoroughly in $CHCl_3$ to generate a hydrophobic surface.

Characterization. FT-IR spectra were recorded with a Mattson spectrometer by mixing the molecules in the KBr matrix or drop casting methylene chloride solution on top of the KBr window. ^{1}H and ^{13}C spectra were recorded with a Bruker 500 MHz spectrometer. Chemical shifts are given in parts per million (δ) relative to tetramethylsilane. UV/vis absorption spectra were taken with a Cary 500 scan UV−vis−NIR spectrophotometer. Fluorescence measurements were recorded on a Jobin Yvon Fluorolog3 spectrometer.

Computational Methodology. Quantum-chemical computations provide powerful insights into electronic structure and dynamics in virtually every molecular class. In particular, adiabatic time-dependent density functional theory (TD-DFT) in the Kohn−Sham (KS) form is currently the method of choice for calculating the excited-state structure of large molecular systems.[31−33] DFT combined with the BHandHLYP functional and the 6-31G basis set were used in all simulations. The 6-31G basis set is known to be an efficient blend of accuracy and a manageable size for large conjugated systems,[34] and the BHandHLYP functional, which incorporates 50% exact exchange, eliminates most charge-transfer problems in the excited states that plague other hybrid, semi-local, and pure functionals. These problems are less important for single chromophore modeling, but become extremely severe for molecular assemblies in question. We start our calculations with optimization of ground-state geometries. TD-DFT formalism implemented in the Gaussian 03 program package (Frisch, et al. *Gaussian 03*, revision C.02; Gaussian,

(30) Skotheim, T. A. E. R. L.; Reynolds, J. R. *Handbook of Conducting Polymers*, 2nd ed.; Marcel Dekker: New York, 1998.

(31) Becke, A. D. *J. Chem. Phys.* **1993**, *98*, 5648−5652.
(32) Runge, E.; Gross, E. K. U. *Phys. Rev. Lett.* **1984**, *52*, 997−1000.
(33) Casida, M. E. *Recent Advances in Density-Functional Methods*; Singapore, 1995; Vol. 3.
(34) Masunov, A. M.; Tretiak, S. *J. Phys. Chem. B* **2004**, *108*, 899−907.

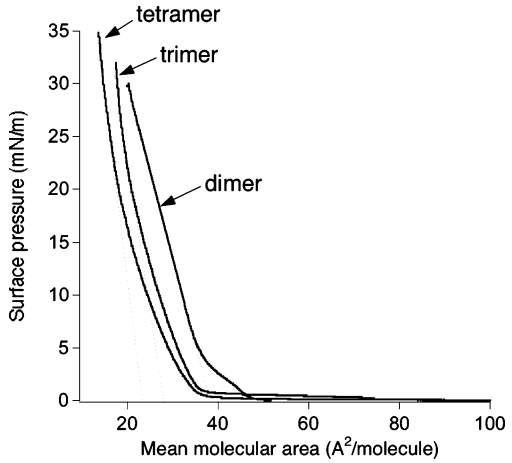

Figure 1. Pressure isotherm of phenylene ethynylene oligomers measured at 25 °C.

Inc.: Wallingford, CT, 2003) was then used to calculate the excited-state electronic structure. To model the solvent effects, the electronic structure of the monomers was calculated with the polarizable continuum model (PCM) based on the integral equation formalism (IEF), as implemented in Gaussian 03, using chloroform as a solvent. Solvent-induced trends remained the same when other versions of PCM were used. We also calculated excited states of pairs of the PPE oligomers to obtain insights into the electronic structure of films and interactions due to interchromophore contacts. The molecules were fixed in their BHandHLYP optimized geometries and oriented co-facially a set distance apart.

Results and Discussion

The final structures and their associated properties of functional materials created using self-assembly methods are often governed by the delicate balance between electrostatic forces and noncovalent interactions between molecular building blocks. In this work, a series of molecular building blocks (see Scheme 1) have been synthesized. These molecular building blocks have the following characteristics: (1) tunable noncovalent ($\pi-\pi$) interaction between amphiphiles; the intermolecular interaction increases as the oligomer chain length increases; (2) luminescent chromophores that will allow us to probe the structure and packing density using optical spectroscopy; and (3) identical van der Waals (VDW) interaction between amphiphiles; VDW is essentially proportional to the length of the alkyl tail, and for the three amphiphilies used in this study, the alkyl groups attached to the chromophores are the same. These unique features of synthesized structures allow us to isolate the effect of noncovalent interaction on the final properties of the functional nanoassemblies. The 2D structure and packing density of the monolayer at the air−water interface can be determined by the transfer ratio and the pressure isotherm measured at a specific temperature. The UV−vis spectroscopy provides quantitative information about the structure−property relationship at the nanoscale as we construct the 3D materials with the bottom up approach.

Pressure Isotherm. The pressure−area isotherm of dimer, trimer, and tetramer is shown in Figure 1. We call our molecules "dimer", "trimer", and "tetramer" according to the number of the benzene rings in the oligomer. The pressure isotherm of the dimer in the range of 0 mN/m < Π < 3 mN/m exhibits a liquid expanded (LE) phase followed by a phase transition to a liquid-condensed (LC) phase (3 mN/m < Π < 30 mN/m). From the linear part of the LC phase, the mean area per molecule can be obtained by extrapolating the pressure isotherm at LC phase to zero pressure (A_0). The area/molecule (A_0) in a liquid condense state is 37 Å^2/molecule for the dimer, 28 Å^2/molecule for trimer, and 23 Å^2/molecule for tetramer. If we trace the pressure isotherm to the highest surface pressure where the molecules are fully compressed, the corresponding area/molecule is 17, 20, and 23 Å^2/molecule for tetramer, trimer, and dimer, respectively. The intermolecular distance is then calculated to be 4.1, 4.3, and 4.8 Å for tetramer, trimer, and dimer. The intermolecular distance and packing density of these phenylene ethynylene oligomers derived from the *P*−*A* isotherm are consistent with those of the conjugated chromophores such as tolan,[35] azobenzene,[36] and oligothiphene[37] derivatives. The smaller area per molecule with increasing repeat units can be explained by the increasing $\pi-\pi$ interactions between oligomer chromophores at the air−water interface, which then lead to formation of a monolayer LB thin film with higher packing density.

The isotherm hysteresis for dimer, trimer, and tetramer is almost identical for three compression and decompression cycles (figures not shown). These results suggest that they all form a stable monolayer at the air−water interface.

Formation of Multilayer L−B Films on Substrate. After establishing the fact that phenylene ethynylene oligomers form a stable monolayer at the air−water interface, we then transferred the as-formed Langmuir film to a substrate surface and studied the electronic and optical properties. For phenylene ethynylene dimer, trimer, and tetramer, monolayers were compressed at a surface pressure of 30 mN/m and then subsequently transferred onto quartz glass substrate. The multilayer deposition processes were monitored via UV−vis spectroscopy. First, a very good transfer ratio (TR = 0.9 ± 0.1) is observed for dimer in the upward direction. In the downward direction, the transfer ratio is very low (TR = 0.1). Therefore, the films are likely to be Z-type. For trimer, the transfer ratio of the LB film is nearly 1.0 during the down and up cycles, indicating the formation of Y-type films. For tetramer, the transfer ratio is about 0.9 for the down cycles and nearly 0 for the up cycles. The films are likely to be X-type. The UV−vis spectra of the LB multilayer films for the phenylene ethynylene trimer and tetramer are shown in Figure 2. The linear increase of the UV absorbance clearly shows a linear increase in the amount of oligomers deposited onto the substrate with each deposition cycle. The λ_{max} of absorbance red-shift from 300 to 348 nm as the chain length increases is simply due to an increase in conjugation. The electronic coupling between chromophores is also manifested by comparing the UV−vis spectra between solution and LB films as shown in Figure 3.

Figure 3 shows the UV−vis absorption spectrum of phenylene ethynylene dimer, trimer, and tetramer in solution and in the 10-layer LB thin film. For the purpose of better comparison, we overlay the thin film spectra on top of the solution spectra. The absorption spectra for the dimer, trimer, and tetramer solution show sharp peaks at 308, 338, and 348 nm, respectively. The red-shift of UV−vis absorption with increasing number of phenylene ethynylene unit results mainly from the increase in conjugation length. The UV−vis absorption spectra for the multilayer LB films of phenylene ethynylene dimer, trimer, and tetramer are also shown in Figure 3. The absorbance maximum of these LB films is at 309, 323, and 340 nm, respectively. The absorbance maximum for the dimer thin film is almost identical to that of the solution. However, trimer and tetramer LB films exhibit a slight blue-shift of 15 and 9 nm, respectively. This

(35) Mavridis, A.; Moustakalimavridis, I. *Acta Crystallogr., Sect. B* **1977**, *33*, 3612−3615.
(36) Aoki, K.; Nakagawa, M.; Seki, T.; Ichimura, K. *Bull. Chem. Soc. Jpn.* **2002**, *75*, 2533−2539.
(37) Bredas, J. L.; Calbert, J. P.; Da Silva, D. A.; Cornil, J. *Proc. Natl. Acad. Sci. U.S.A.* **2002**, *99*, 5804−5809.

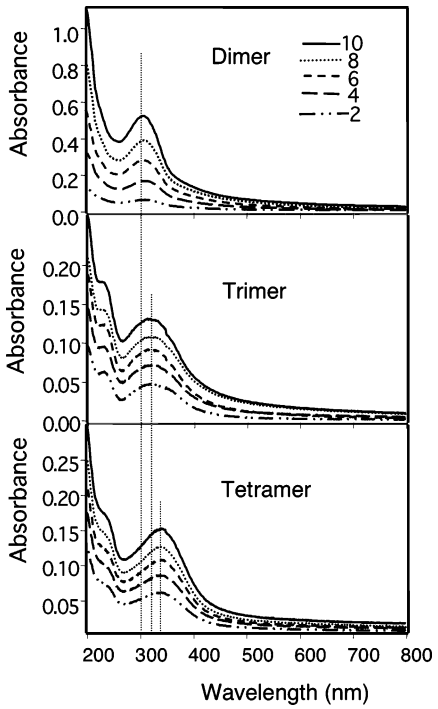

Figure 2. Plot of UV−vis spectra of multilayer LB films as a function of layer number.

trend is consistent with H-aggregate formation in the LB films. However, several other factors such as disorder may account for the observed weak blue-shift as well. Careful analysis of the emission profiles and ultrafast time-resolved spectroscopic probes should help to unambiguously identify the presence of H-aggregates in LB films.[38] Furthermore, comparing the spectra between the solution and LB films, we observe broader absorbance peaks for the thin film presumably due to electronic interactions between conjugated chromophores. Such broadening and the lack of vibrational replicas indicate a strong inhomogeneous energetic distribution due to interchromophore interactions and disorder of the films. The observed electronic couplings result from close intermolecular contacts. Imperfect molecular packing, solvent environment, and molecular conformations lead to energetic disorder, which may emphasize H-aggregate signatures.[39] To better understand the effect of surface pressure on the properties of the final L−B films, we construct LB films at two different surface pressures (15 and 30 mN/m), and the results are shown in Figure 4. In this figure, we can clearly observe that a greater amount (∼60%) of trimer was deposited onto the substrate in higher surface pressure presumably due to a more densely packed layer structure. However, the electronic spectra of trimer LB films deposited at different surface pressure are basically identical. We suspect this similarity in UV−vis spectra at two surface pressures could be due to that the surface pressure of 15 mN/m is already close to the transition point from the liquid expanded state to the liquid condensed state. Another possible explanation can be due to aggregate formation during the early stage of compression. The later compression only brings aggregates together without causing the increase of the chromophore interaction.

Photoluminescence. The emission properties of the solutions and LB films of the dimer, trimer, and tetramer are shown in Figure 5. As expected, due to the increased conjugation length from dimer to tetramer, the observed emission maximum of

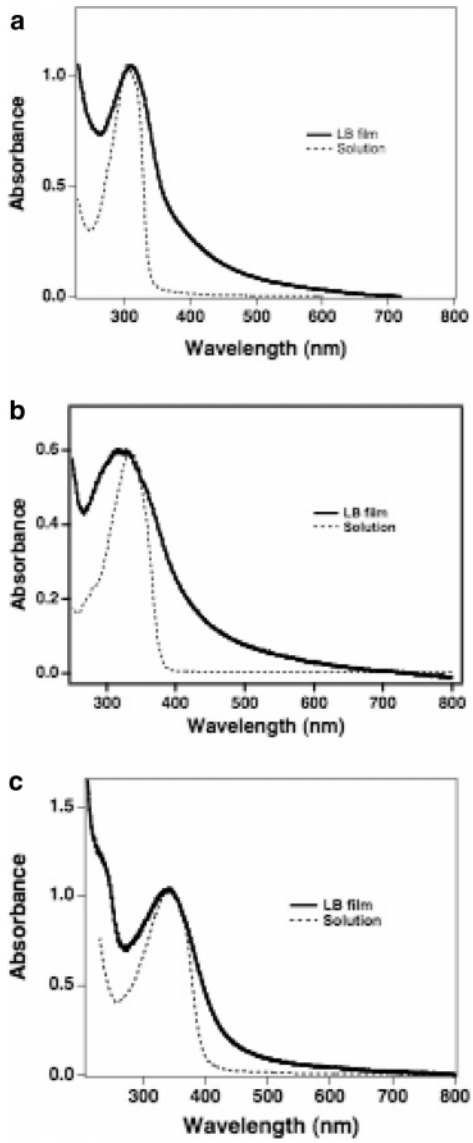

Figure 3. UV−vis spectra of phenylene ethynylene oligomers in solutions and on LB films: (a) dimer, (b) trimer, and (c) tetramer.

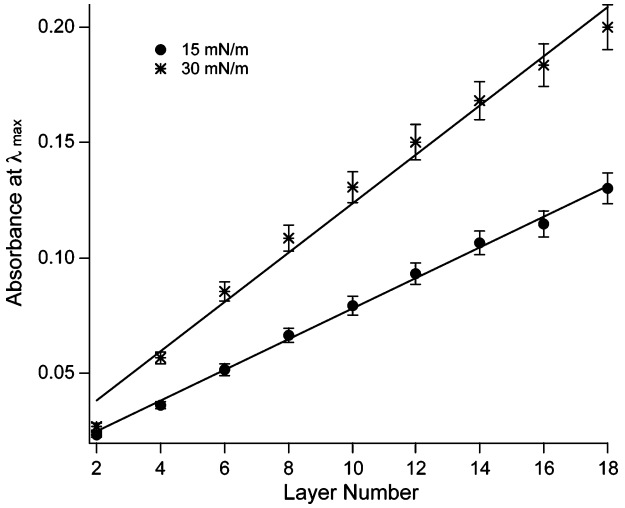

Figure 4. Plot of absorbance of LB films as a function of layer number in two different surface pressures.

solution is red-shifted from 370, 430, to 450 nm. The emission spectra of LB films appear similar to that of the solution except that the intensity of emission spectra of LB films decreased

(38) Siddiqui, S.; Spano, F. C. *Chem. Phys. Lett.* **1999**, *308*, 99−105.
(39) Knox, R. S. *J. Phys. Chem.* **1994**, *98*, 7270−7273.

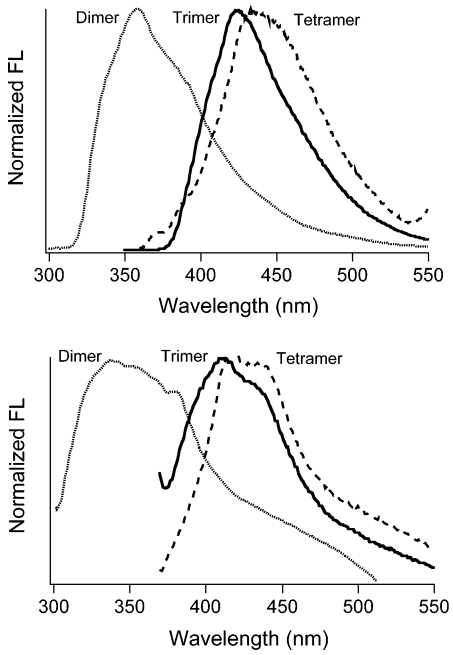

Figure 5. Photoluminescence of OPE solutions (a) and multilayer LB films (b).

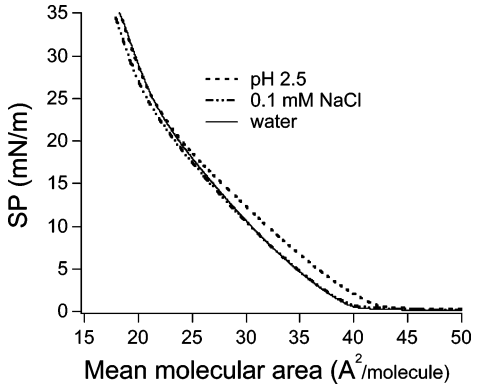

Figure 6. Pressure isotherm of phenylene ethynylene trimer under various experimental conditions.

dramatically. For example, the quantum efficiency of a diluted trimer solution is determined to be 28% using coumarin 450 as standard, and the quantum efficiency of the LB film is estimated to be ~1%, significantly lower than that of the solution. This significant decrease in the quantum efficiency is likely due to the self-quenching resulting from defects, excimers, and exciplexes formed at close contact between chromophores. The efficient quenching is also an indication of molecules being densely packed within the LB films.

Enhanced packing density and aggregate formation have a huge impact on the final optical properties of the LB multilayer thin films.The packing density of OPE monolayer at the air−water interface can be easily altered by varying the experimental parameters. Figure 6 shows the pressure isotherms of OPE trimer measured in various experimental conditions. In this particular experiment, we vary the subphase condition by adding salt or acid to the subphase to vary the charge density on the hydrophilic headgroups. It is clearly seen that the pressure isotherm under the 0.1 M NaCl overlaps nicely with the pressure isotherm obtained in pure water in both the gas phase and the liquid expanded state. However, these two curves diverge as they move into the liquid condensed state. This very interesting result can be explained in that the salt addition does not cause significant

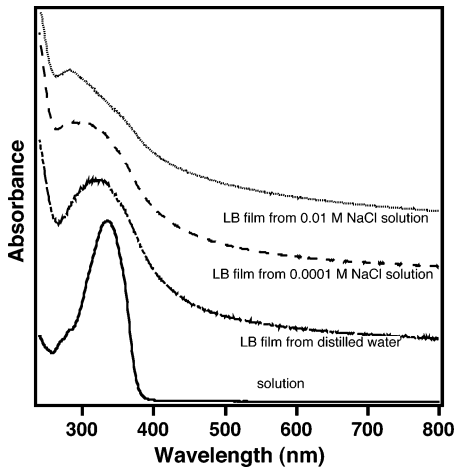

Figure 7. UV−vis spectra of OPE trimer in solution and its LB films prepared under various experimental conditions.

changes in the packing density until the molecules come in close contact with each other. The unfavorable charge repulsion between amine headgroups (the pK_a of the OPE trimer is estimated to be ~4.6) is reduced as the salt serves to buffer the charged headgroups. The packing density of OPE trimer at the liquid condensed state is therefore increased because of this reduced charge repulsion. As the pH of the subphase is changed to 2.5, we expect the headgroup to be completely charged, and therefore increase the overall charge of amine headgroups at the air−water interface. The pressure isotherm carried out at pH = 2.5 shows an early rise in the liquid expanded states; that is, the molecules establish contact with each other at a larger surface area. This can be understood as the charges on the amine headgroups result in a larger solvation volume that causes OPEs to interact with each other at a greater distance. However, the liquid condensed state overlaps nicely with the pressure isotherm obtained when the subphase is pure water. This result indicates that final packing density in the liquid condensed states is not affected by the pH value. The above results are also consistent with a previous report,[40] which shows that an increasing ionic repulsion between hydrophilic headgroups results in the contact between molecules at a greater distance with the final packing density (area/molecules) remaining the same. Impact of packing density on the electronic properties of the OPE monolayer at the air−water interface is also manifested in the absorbance spectra of L−B films upon transferring the monolayer structure to a substrate. Figure 7 show the UV−vis spectra of L−B thin films prepared from subphase with various ionic strength. In this figure, we can clearly observe a monotonic blue-shift as the OPE molecules evolve from molecular dispersion to thin film prepared under various conditions. The blue-shift of the UV−vis spectra supports our conjecture on formation of H-aggregates. As we increase the ionic strength of the subphase, the absorbance of L−B films shifts further to the blue, indicative of a strong intermolecular interaction in the liquid condensed state. This result is consistent with pressure isotherm data, which show that the presence of 0.1 mM in the subphase results in a higher packing density (smaller surface area/molecules). From the above results, we can also conclude that varying the molecular structure as well as experimental parameters such as the ionic strength of the subphase can fine-tune the intermolecular interaction that will lead to monolayer structure with various electronic and optical properties.

Molecular Simulations of PPE Oligomers. To better understand how molecular packing affects electronic structure and optical spectra of OPE LB films, we have performed a series

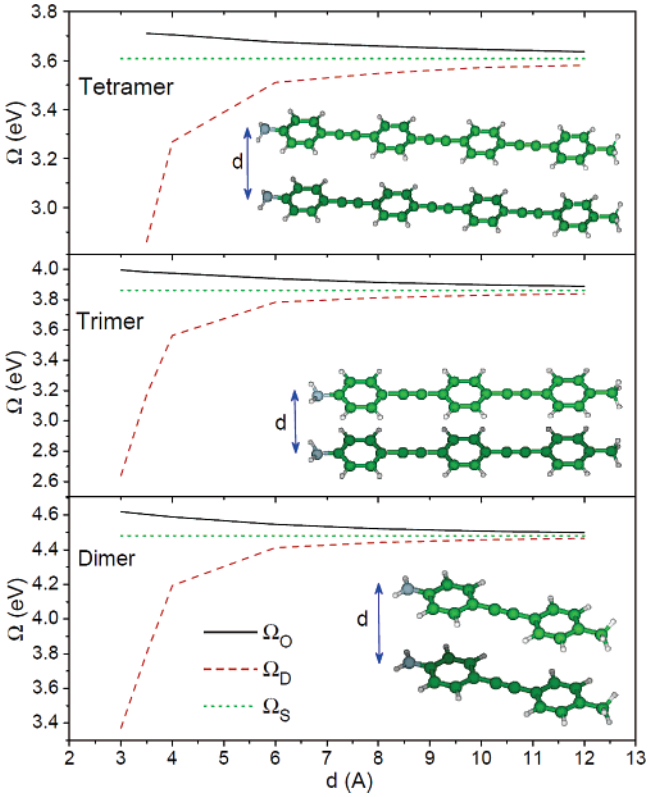

Figure 8. Optically active (Ω_O) and dark (Ω_D) excitation energies (Davydov's pair) for pairs of phenylene ethynylene oligomers in comparison with excitation energy (Ω_S) of a single molecule plotted as a function of intermolecular separation *d*. Insets show parallel orientation of calculated molecular pairs.

of quantum-chemical calculations of dimer, trimer, and tetramer molecules. The purpose of these simulations is to gain insight into the packing, solvent effects, and the qualitative prediction of the shifting of the absorption peaks observed in the UV−visible spectra. In our calculations, methyl groups have replaced the long carbon chains, as these chains should not drastically affect the excited states of $\pi-\pi^*$ character.

Using the BHandHLYP functional and the 6-31G basis set, we first optimized gas-phase single-molecule atomic positions. These structures were then used for solvent effects and molecular pair calculations. In particular, to construct the molecular pairs, the coordinates for two molecules were placed on top of each other, and one chromophore was shifted to a fixed intermolecular spacing perpendicular to the phenyl rings.

Intermolecular aggregation within 2D assemblies can lead to two arrangements for adjacent chromophores aligned parallel to each other. "Head-to-head" and "tail-to-tail" arrangements of the dipoles lead to so-called H-aggregates. Their optical absorption spectra display prominent spectral blue-shifts in the absorbance as compared to the monomeric units. On the other hand, J-aggregates are formed when dipoles are arranged in a "head-to-tail" configuration, leading to red-shifts in the linear absorption. These spectral shifts can be readily rationalized within Davydov's excitonic model,[41−43] where aggregation of chromophores results

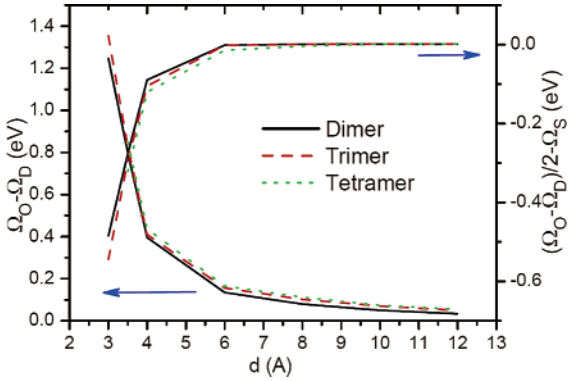

Figure 9. Excited-state level splitting (left) and deviation of the median value of the Davydov's pair from excitation energy of a single molecule (right) for pairs of phenylene ethynylene oligomers shown in Figure 8 plotted as a function of intermolecular separation *d*.

in the delocalized electronic states being coherent superpositions of the monomer's wave functions. For example, upon parallel orientation of the molecular pair, the monomer's optically active excited state splits into two (Davydov's pair). The splitting magnitude reflects an interaction between the chromophores. The red-shifted state would be optically forbidden, whereas the blue-shifted state is optically allowed retaining all of the oscillator strength on the parent chromophores. Figure 8 shows splitting of the first optical state into a blue-shifted optically active state and a lower energy dark state with zero oscillator strength as a function of intermolecular separation. The splitting becomes slightly larger for larger chromophores and dramatically grows as the distance between molecules is reduced as illustrated in Figure 9 (left). The optical state is blue-shifted relative to the isolated molecule limit when the phenylene ethynylene oligomers are packed into a film. This is the key signature of H-aggregation. While these results are calculated for pairs of molecules, the underlying H-aggregation will persist in the film, but the actual level splitting will approximately double according to Hückel's theory. In the ideal case, when the molecules have electrostatic interactions only, the Davydov's states split equally up and down from the isolated molecule limit. This is the case for large intermolecular distances (see Figure 8). Once the chromophores start approaching each other, their wave functions start to overlap and the lowest state shifts further to the red due to strong through-space interactions.[44,45] This deviation from the median level plotted in Figure 9 (right) can be also clearly seen from Figure 8. The Dexter contribution is larger for longer chains (Figure 9, right), which reflects stronger $\pi-\pi^*$ interactions due to tighter packing in the films.

Table 1 summarizes computed spectroscopic observables for the excited states and compares them to experimental values. Calculated excitation energies lie within 0.2 eV of experimental data, which is a typical accuracy expected from hybrid TD-DFT approaches. Overall, the theory well reproduces observed experimental trends. The chloroform solvatochromic shifts are moderate, about 0.1 eV to the red for all molecules. The theoretical results show a blue-shift in the aggregates relative to the isolated

Table 1. Calculated Excitation Energies of a Single Molecule (Ω_S) and a Pair (Ω_O), and Respective Experimental Values Taken at Maximal Absorption from Figure 3

	theory (Ω_S, eV)		experiment (λ_{max}, eV)		theory, pair in vacuo (Ω_O, eV)		
	in vacuo	solvent	solvent	film	4 Å	6 Å	8 Å
dimer	4.48	4.33	4.1	4.08	4.59	4.55	4.52
trimer	3.86	3.74	3.8	3.95	3.97	3.94	3.91
tetramer	3.61	3.51	3.6	3.64	3.71	3.68	3.66

molecules. Notably, this shift deflects delicate interplay between electrostatic (upward) and through-space (downward) interactions. For example, it decreases for the largest oligomer (tetramer) due to stronger $\pi-\pi^*$ overlap. This allows us to rationalize the observed experimental trend for a large H-aggregate blue-shift in the trimer. Dimer films do not have tight packing and, therefore, sufficient intermolecular interactions, whereas closely packed tetramer films have strong $\pi-\pi^*$ interactions leading to red-shifts.

Conclusion

In this contribution, we have achieved the synthesis and characterization of a series of phenylene ethynylene amphiphiles and their L−B thin films. We have shown that by tailored synthesis of molecular building blocks with varying noncovalent interaction, we can obtain the L−B multilayer thin films with tunable packing density and optical properties. The packing density is the end result of a delicate balance between noncovalent interactions that involved electrostatic, $\pi-\pi$ interaction, and dipole−dipole interactions. We have further demonstrated that we can fine-tune the intermolecular interaction by varying the experimental parameters such as ionic strength and pH value of the subphase, leading to a monolayer structure with various electronic and optical properties. The results of quantum-chemical calculations support experimental findings, rationalize observed trends, and validate our results. Understanding achieved through the modeling work also shows promise in predicting the electronic and optical properties of the phenylene ethynylene self-assemblies.

Acknowledgment. We are grateful for the financial support from the Laboratory Directed Research and Development (LDRD) fund and the Office of Science (DOE). Partial support from the Cross Enterprise Technology Development Program of the National Aeronautics and Space Administration (NASA) is also greatly appreciated.

LA060914K

(40) Oishi, Y.; Takashima, Y.; Suehiro, K.; Kajiyama, T. *Langmuir* **1997**, *13*, 2527.
(41) Cossi, M.; Barone, V. *J. Chem. Phys.* **2001**, *115*, 4708−17.
(42) Silinish, E. A.; Capek, V. *Organic Molecular Crystals*; American Institute of Physics: New York, 1994.
(43) Pope, M.; Swenberg, C. E. Clarendon Press: New York, 1982.
(44) Tretiak, S.; Middleton, C.; Chernyak, V.; Mukamel, S. *J. Phys. Chem. B* **2000**, *104*, 9540−9553.
(45) Krueger, B. P.; Scholes, G. D.; Fleming, G. R. *J. Phys. Chem. B* **1998**, *102*, 5378−5386.